Phonon confinement effects in the Raman spectrum of nanodiamond

S. Osswald,[1,*] V. N. Mochalin,[1] M. Havel,[1,†] G. Yushin,[2] and Y. Gogotsi[1,‡]
[1]*Department of Materials Science and Engineering and A. J. Drexel Nanotechnology Institute, Drexel University, Philadelphia, Pennsylvania 19104, USA*
[2]*Department of Materials Science and Engineering, Georgia Institute of Technology, 771 Ferst Drive, N.W., Atlanta, Georgia 30332-0245, USA*
(Received 10 May 2009; revised manuscript received 26 July 2009; published 18 August 2009)

Nanodiamonds (ND) exhibit unique properties due to their small size and high surface-to-volume ratio compared to bulk diamonds. A reduction in crystal size also affects ND Raman spectra. The confinement of optical phonons in nanocrystals (<10 nm) results in asymmetrically broadened Raman lines, which are shifted toward lower wavenumbers. The phonon confinement model (PCM) relates the observed changes in the Raman spectra to the crystal size and can be used for size characterization at the nanoscale. While the PCM was successfully applied to a variety of materials including Si and BN, results remained unsatisfactory in the case of ND. In order to improve the agreement between the predictions of the model and experimental Raman spectra of ND, effects such as crystal size distribution, lattice defects, and the energy dispersion of the phonon modes were taken into consideration and incorporated into the PCM. This work has shown that phonon wave vectors from small vibrational domains lead to a broad shoulder peak at ~1250 cm^{-1}, that is often observed in the Raman spectrum of ND.

DOI: 10.1103/PhysRevB.80.075419 PACS number(s): 63.22.−m, 61.46.−w, 81.07.−b

I. INTRODUCTION

Since the discovery of fullerenes in 1985, researchers have put much effort into studying carbon nanoparticles at the nanometer scale. Today, nanostructured carbons are available in various forms such as powders, colloids, thin films, and composites.[1] Raman spectroscopy has become a powerful tool to analyze carbon nanomaterials including nanotubes, fullerenes, nanodiamond (ND), carbon onions, and graphene.[2] It provides information on structure, composition, and homogeneity of a material, and identifies bonding and surface functionalities.[3,4] It can also be used to estimate temperature and stress in the samples.[5] Carbon allotropes such as graphite[6,7] or diamond[8,9] show unique Raman signals, thus allowing a fast and straightforward identification. The interpretation of Raman spectra of nanostructures is, however, more complex.[2] As the dimensions of a material are reduced, the increasing surface/volume ratio can result in dramatic changes in properties, especially when entering the lower nanometer range. A significant decrease in crystal size also affects lattice vibrations and leads to changes in the Raman spectrum. While numerous and thorough studies have been conducted on all kinds of graphitic carbons, Raman spectra of ND are still not completely understood. For example, only recently the ~1140 cm^{-1} peak in the spectrum of chemically vapor deposited (CVD) ND was assigned to polyacetylene vibrations[10] and the ~1640 cm^{-1} peak in the spectrum of detonation ND was associated with hydroxyl group OH bend vibrations.[11]

The crystal structure of diamond consists of two interpenetrating face-centered cubic sublattices with eight atoms per unit cell, leading to three optical and three acoustic phonon modes.[12] The phonons propagate into the crystal lattice with an energy that depends on their associated wave vectors in the Brillouin zone (BZ). As a consequence of momentum conservation and because the BZ of an infinite perfect crystal is much larger ($|\boldsymbol{k}_{BZ}| \approx 10^8$ cm^{-1}) than the largest possible scattering vector using conventional Raman spectroscopy in backscattering geometry ($|\boldsymbol{k}_S| \approx 6 \cdot 10^4$ cm^{-1} for 325 nm excitation), only phonon modes from the center of the BZ ($|\boldsymbol{q}| = |\boldsymbol{k}_S| / |\boldsymbol{k}_{BZ}| \approx 0$) can contribute to the first-order Raman spectrum.[5,13] However, phonons are confined by defects or grain boundaries in finite crystals and the $\boldsymbol{q}=0$ selection rule is released. The resulting changes in the Raman spectra can be used to estimate the crystal dimensions of nanostructures.

Size measurements using Raman spectroscopy are based on the analysis of the Raman frequency and Raman peak shape. Unfortunately, a precise *ab initio* determination of the vibration dynamics in nanostructures is currently restricted to crystals below 1 nm due to computational power requirements. Therefore, several semiempirical models have been developed in order to relate the observed changes in the Raman spectrum to the crystal size including the phonon confinement model[14,15] (PCM) and the elastic sphere model[16,17] (ESM). A review of existing confinement models was recently given by Arora *et al.*[18]

A. Phonon confinement model

Richter *et al.*[15] and Nemanich *et al.*[14] independently investigated how the uncertainty of the wave vector will affect the Raman lines and suggested a PCM that correlates the observed changes with the crystal size. A plane-wave-like phonon cannot exist within a nanocrystal because the phonon cannot propagate beyond the boundary. Therefore, the wave function of the phonon must decay to a very small value at the crystal boundary. A weighting function (confinement function) accounts for decay of the wave function and contributions from phonons away from the center of the BZ. The wave vector uncertainty associated with a vibration is given by $\Delta q = \pi / L$, where $q = |\boldsymbol{q}|$ and L is the crystal size. It should be mentioned that this approximation becomes less valid for

strongly confined phonons.[18] The size of BZ boundary wave vector is $|k_{BZ}|=\pi/a$, where a is the lattice constant of the crystal. For example, a 20 nm diamond crystal ($a=0.3567$ nm) would cause an uncertainty of $\Delta q \approx 2\%$ with respect to the phonon wave vector of the zone-center vibration and the size of the BZ.

Assuming one-phonon zone-center Raman scattering, the first-order Raman line can be constructed by superposition of Lorentzian peaks centered at the frequency ω and weighted by the uncertainty of the wave vector (see Ref. 15)

$$I(\omega) \cong \int \frac{|C(\boldsymbol{q}_0,\boldsymbol{q})|^2}{[\omega-\omega(\boldsymbol{q})]^2-(\Gamma_0/2)^2} d^3\boldsymbol{q} \tag{1}$$

where $C(\boldsymbol{q}_0,\boldsymbol{q})$ are the Fourier transform coefficients of the confinement function,[15] and $\omega(\boldsymbol{q})$ and Γ_0 are the phonon-dispersion relation and the natural line width of the zone-center Raman line, respectively. $\boldsymbol{q}_0$ is the wave vector of a phonon in an infinite crystal. The predicted Raman line is asymmetrically broadened and shifted to lower wavenumbers as crystal size decreases. Equation (1) accurately describes confinement effects in Si,[19–21] BN,[14] and GaAs.[22,23]

B. Raman spectrum of nanodiamond powders

The first-order Raman spectrum of a perfect bulk single-crystal diamond displays one triple-degenerated Raman line at 1332 cm^{-1} with a full-width at half-maximum (FWHM) of $\sim 1-2$ cm^{-1}.[9] ND films and powders show additional peaks that result from grain boundaries, structural defects, surface-related contributions, and impurities (e.g., amorphous and graphitic carbon).[24] As a consequence, Raman spectra of ND become quite complex and depend on synthesis technique, structure, surface chemistry, and purity of the samples.

Position, intensity, and number of Raman peaks change with changing sp^3/sp^2 ratio [Fig. 1(a)]. The Raman spectra of ND powders with low-sp^3 and high-sp^2 UD50 carbon content are dominated by the D and G bands of graphitic carbon and exhibit only a weak or no diamond signal. With increasing sp^3 content, the intensity of the diamond peak increases, while the D band weakens. The diamond peak is broadened (FWHM >30 cm^{-1}) and down-shifted (~ 1326 cm^{-1}) with respect to bulk diamond, with a shoulder at ~ 1250 cm^{-1}.[25–28] Spectral features between 1500 and 1800 cm^{-1} are more complex and three peaks at ~ 1590, ~ 1640, and ~ 1740 cm^{-1} have recently been assigned to sp^2 carbon, O-H, and C=O groups, respectively.[11] It should be noted that shape and intensity of the Raman peaks also change for different excitation wavelengths, due to different resonance conditions of sp^2 and sp^3 carbon.[24]

Ager *et al.*[29] tried to relate confinement-induced changes in the Raman spectrum of diamond to the crystal size. Following the approach of Richter *et al.*,[15] they estimated the crystal size by reducing the three-dimensional integration in Eq. (1) to a one-dimensional (1D) integration over a spherical BZ using an averaged one-dimensional dispersion curve of the form $\omega(q)=A+B\cdot\cos(q\pi)$, where $A=1241.25$ cm^{-1} and $B=91.25$ cm^{-1}. Assuming a Gaussian confinement function, they calculated the Raman intensity according to:

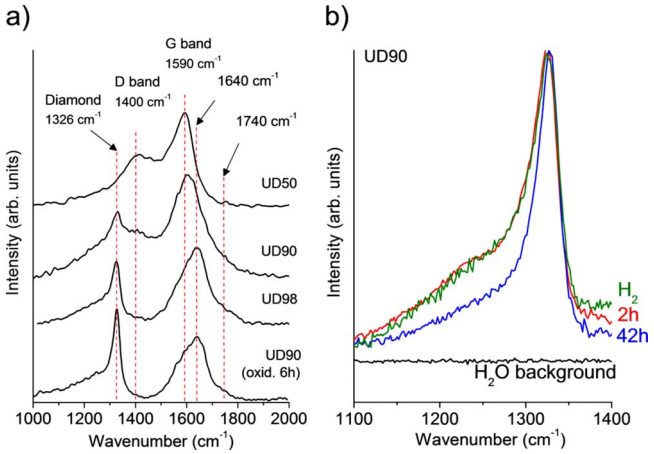

FIG. 1. (Color online) (a) Raman spectra of different ND powders with increasing sp^3 contents from less than 30% in the top (UD 50) spectrum to more than 95% in the lower spectrum (UD90 oxidized for 6h). Intensities were normalized to the G band intensity at 1590 cm^{-1}. (b) Diamond Raman peak recorded after H_2 annealing and oxidation in air for 2 and 42 h, measured in water. All spectra were recorded using the 325-nm laser excitation.

$$I(\omega) \cong \int_0^1 \frac{\exp(-q^2L^2/4)\cdot 4\pi q^2}{[\omega-\omega(q)]^2-(\Gamma_0/2)^2} dq. \tag{2}$$

However, their results showed a rather poor agreement with experimental Raman spectra. In contradiction to the PCM, they observed an up-shift in the diamond peak with decreasing crystal size, suggesting other mechanisms, such as stress, affecting the Raman line.[30,31] Mismatch of the crystal lattices of CVD diamond and the substrate leads to changes in line shape and position as a function of the stress direction.[32,33] Phonon confinement and stress simultaneously affect the Raman spectrum of ND films, thus making size measurements using the PCM difficult.[29,33]

Yoshikawa *et al.*[34] focused their analysis on ND powders synthesized by detonation of explosives. Using the approach of Ager *et al.* they modeled the Raman line of a 5.5-nm diamond particle (average crystal size in detonation ND). Although their results are in better agreement with the experimental data compared to ND films, the accuracy was still unsatisfactory.

In most of the former studies, only individual ND samples were analyzed and compared to microcrystalline or bulk diamond. However, in order to verify the confinement-related changes in the Raman spectra and to improve the reliability of the model, studies on samples with different crystal sizes below $L=20$ nm, where confinement effects are significant and easier to observe, are required.

Another crucial factor is the excitation wavelength used in Raman analysis of ND samples. Raman spectra recorded from ND samples using visible laser excitation are often dominated by the features of nondiamond species. Visible light may produce strong fluorescence which overlaps with the Raman spectra, requiring extensive base-line corrections or background subtraction. In both cases, an exact determi-

nation of the diamond peak shape, position, and width is difficult if not impossible.

The importance of adopting Raman spectroscopy for size measurements of nanostructures is emphasized by the fact that common techniques such as dynamic light scattering or gas sorption, used for measuring the particle size of powders, cannot provide reliable data on ND crystal size due to strong agglomeration typically observed for nanomaterials. Although high-resolution transmission electron microscopy (HRTEM) directly probes the actual crystal size, it is expensive and lacks statistical reliability, because of the very small sample volume being studied.[35] Crystal size derived from x-ray diffraction (XRD) is based on constructive interference and can become inaccurate for samples that contain both large and small crystals.[35,36]

Currently, Raman spectroscopy cannot be used to quantitatively measure the average crystal size in ND powders. However, with a better understanding of phonon confinement effects in the Raman spectra, Raman spectroscopy may be adopted to measure crystal size and changes in the size distribution. In this study, we investigate the effects of crystal size, defect concentration, and crystal size distribution on the ultraviolet (UV) Raman spectra of ND and modify the PCM in order to account for these contributions.

II. EXPERIMENTAL

A. Materials

ND powders of UD50, UD90, and UD98 grades were supplied by NanoBlox, Inc. (USA). Black UD50 is the raw detonation soot and UD90 and UD98 were produced by acid purification. Oxidative purification of UD90 (in air) was conducted under isothermal conditions (420 °C) in a rotating tube furnace.[27] The ND powders used for crystal size measurement were produced from UD90 by oxidation in air for 2, 6, 17, 26, and 42 h at 430 °C.[35] High-temperature hydrogenation (2 h at 800 °C) was done with "ultrahigh-purity" hydrogen supplied by Air Gas (USA).[37]

B. Characterization

UV Raman analysis was performed in backscattering geometry using a Renishaw 2000 Raman microspectrometer equipped with a high-sensitivity ultralow noise RenCam charge-coupled device (CCD) detector. Spectra were recorded using a 325-nm HeCd laser (1300 W/cm^2), 2400 l/mm grating, 15×/40× objective, and a 100 cm^{-1} cutoff notch filter. UV laser excitation minimizes contributions from nondiamond species to the Raman spectra and allows an unadulterated characterization of the diamond line. While UV laser excitation provides strong enhancement of the diamond signal, it can damage the sample and change the composition by laser-induced burn-off. Our experiments showed that a laser power as low as 0.4 mW (514-nm excitation wavelength), focused to a spot size of ~20 μm (50× objective), can heat a carbon sample instantaneously up to 350 °C, which is within the range of oxidation temperatures of amorphous sp^2 carbon.[27,38,39] Such high temperatures are the result of a poor heat transfer between nanoparticles.[40] Even if the laser heating is not enough to induce oxidation, changes in the position and shape of the Raman lines are expected to occur,[33] interfering with confinement effects. To minimize heating and avoid laser-induced changes in the sample, all Raman measurements were performed in water. Although O-H groups were found to contribute to the Raman spectrum of ND,[11] they do not affect the Raman intensity in the range 1100–1400 cm^{-1} [Fig. 1(b)].

High-resolution transmission electron microscopy images of ND powders were produced with JEOL 2010F at accelerating voltage of 100 and 200 kV. HRTEM samples were prepared by dispersing ND powders in isopropyl alcohol over a copper grid coated with a lacy carbon film.

C. Computations

The best-fit parameters of Eq. (2) for experimental Raman spectra of ND powders with different particle size distributions were found by nonlinear multivariable constrained optimization procedure implemented as a MATLAB code.

III. RESULTS AND DISCUSSION

A. Raman spectra of oxidized nanodiamond

In order to study phonon confinement effects and better understand size-related changes in the Raman spectra of ND, we produced ND powders with different average crystal sizes using oxidation for 2, 6, 17, 26, and 42 h at 430 °C in air.[35] The corresponding average crystal sizes have been determined by x-ray diffraction using the Williamson-Hall analysis and were 4.8, 5.2, 5.5, 6.5, and 7.0 nm, respectively.[35]

We first measured the ND crystal size of the oxidized powders using the models of Ager *et al.*[29] and Yoshikawa *et al.*[34] The Raman spectra were calculated following Eq. (2). The approach of Yoshikawa *et al.* accounts for size-related changes in the phonon lifetime ($\Gamma > \Gamma_0$), leading to larger downshift and higher-peak asymmetry compared to Ager *et al.* [Fig. 2(a)]. Although differences between the models are small for larger crystals, they become significant for crystal sizes below 10 nm and are therefore important for size characterization of ND powders [Fig. 2(a)]. The confinement-induced asymmetry of the Raman peak decreases with increasing oxidation time, leading to a narrower diamond line [Fig. 1(b)]. It is important to note that the intensity of the shoulder around ~1250 cm^{-1} also decreases with oxidation time. This shoulder results directly from the ND crystals and their confined size and does not depend on surface chemistry of ND [Fig. 1(b)].[35]

B. Size measurements using Raman spectroscopy

Since both models do not account for the shoulder at ~1250 cm^{-1}, we only fit experimental data in the range of 1290–1360 cm^{-1} [circles in Fig. 2(b)]. The fits and the corresponding crystal sizes for the ND powder oxidized for 2 h at 430 °C, referred to as ND(2h), are shown in Fig. 2(b). Although both models lead to crystal sizes comparable to that obtained from XRD in the 3–5 nm range, the agreement between calculated and recorded Raman spectra is unsatis-

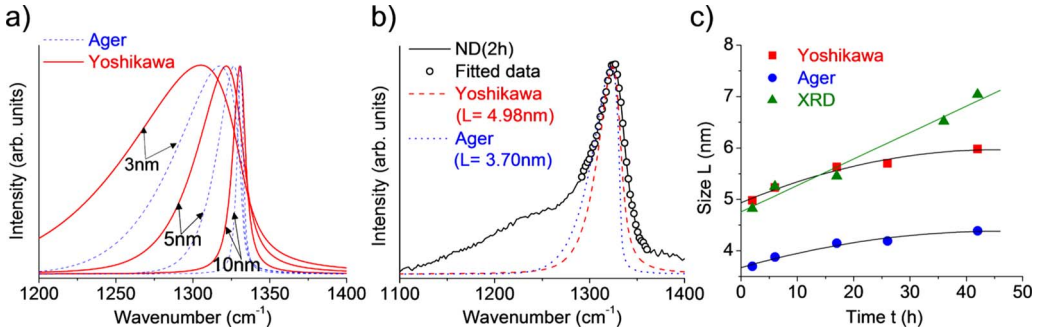

FIG. 2. (Color online) (a) Raman spectra for 3-, 5-, and 10-nm diamond crystals calculated using the approach of Ager *et al.* and Yoshikawa *et al.* (b) Raman spectrum of ND powder oxidized for 2 h at 430 °C in air and the corresponding peak fit. Data used for peak fitting are indicated by the circles. (c) Calculated crystal size for ND powders oxidized for 2, 6, 17, 26, and 42 h at 430 °C. X-ray diffraction data is shown for comparison.

factory. The calculated crystal sizes of all oxidized powders are presented in Fig. 2(c), in comparison to XRD results. While Ager's model leads to slightly smaller sizes, both models show an increase in crystal size with increasing oxidation time, in agreement with XRD data. Crystal sizes calculated using Yoshikawa's model closely match the values obtained from XRD analysis for 2, 6, and 17 h [Fig. 2(c)], but are lower for longer oxidation times (>20 h). Changes in crystal size L (in nm) with increasing oxidation time t (in h), as measured by Raman spectroscopy, can be fit using a second-order polynomial

$$L = C_1 \cdot t^2 + C_2 \cdot t + C_3, \tag{3}$$

where $C_1 = -5.0 \cdot 10^{-4}$ nm/h^2, $C_2 = 0.04$ nm/h, and $C_3 = 4.94$ nm for Yoshikawa's, and $C_1 = -3.4 \cdot 10^{-4}$ nm/h^2, $C_2 = 0.03$ nm/h, and $C_3 = 3.68$ nm for Ager's model, respectively.

It should be noted that the measured sizes represent average values. HRTEM characterization of the oxidized ND powders revealed a broad size distribution, showing ND crystals of 3–20 nm or larger (see Ref. 35). Faster oxidation of small ND crystals leads to an up-shift in the average crystal size after oxidation. The discrepancies between the sizes measured by XRD and Raman spectroscopy observed for longer oxidation times (>20 h) may result from the difference in the effective scattering cross section of both techniques with respect to the increasing contribution of larger ND crystals. The sensitivity toward defects and changes in lattice spacing is also expected to be different for these techniques.

C. Changes in phonon lifetime

In their model, Yoshikawa *et al.*[41] assumed the line width Γ (FWHM) of the diamond peak, representing the phonon lifetime, to be dependent on the crystal-size L. Their experiments on microcrystalline diamond revealed a broadening of the diamond peak with decreasing crystal size

$$\Gamma = A + \frac{B}{L}, \tag{4}$$

where Γ and L are the FWHM (in cm^{-1}) and ND crystal size (in nm), respectively. The parameter B is material specific and related to the size dependency of the FWHM. The parameter A represents the FWHM of bulk diamond, but includes the spectrometer-related line broadening. The parameters determined by Yoshikawa *et al.*[41] are $A = 2.990$ cm^{-1} and $B = 145.74$. Sun *et al.* used a similar approach and found $A = 9.45$ cm^{-1} and $B = 275.73$.[42] However, these results were obtained by using microcrystalline diamond and might not hold at the nanoscale. In order to test the reliability of the reported size dependency, we set Γ as fitting parameter, in addition to the crystal-size L. The obtained results are presented in Fig. 3. It can be seen that optimization of both L and Γ leads to a better agreement between the calculated and

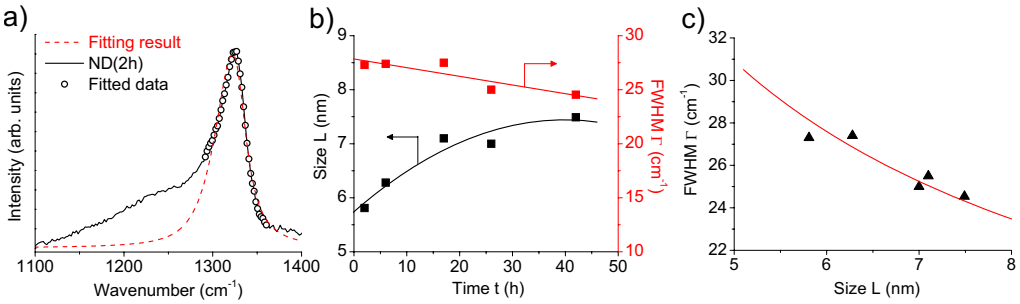

FIG. 3. (Color online) (a) Raman spectrum of oxidized ND (2 h at 430 °C) fitted using peak width Γ (FWHM) and crystal size L as fitting parameters. Similar fits were used for all oxidized ND powders to determine (b) changes in Γ and L as a function of oxidation time and (c) the relationship between both parameters.

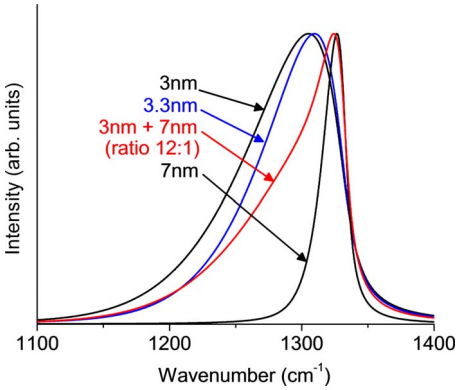

FIG. 4. (Color online) Calculated Raman spectra for different ND crystal sizes in comparison to that of a sample containing a bimodal size distribution.

the measured Raman spectra, in particular at higher frequencies [compare Figs. 2(b) and 3(a)]. The values of L and Γ of all oxidized ND powders are shown in Fig. 3(b). As expected, L increases with increasing oxidation time. The time dependency of L (in nm) is well described by Eq. (3) with coefficients $C_1=-1.1\cdot10^{-3}$ nm/h^2 $C_2=0.08$ nm/h, and $C_3=5.74$ nm. The FWHM (in cm^{-1}) decreases linearly with oxidation time

$$\Gamma = D_1 \cdot t + D_2, \tag{5}$$

where D_1 and D_2 are -0.08 cm^{-1}/h and 27.8 cm^{-1}, respectively. The resulting relationship between L and Γ is shown in Fig. 3(c). The data was fitted using Eq. (4), according to the approach suggested by Yoshikawa *et al.*[41] and Sun *et al.*[42] The parameter A was set to 11.0 cm^{-1}. This value corresponds to the FWHM measured for bulk diamond and includes the spectrometer-related line broadening. B was obtained from the fit and found to be 99.66, which is smaller than the values reported by Yoshikawa *et al.* (145.74) (Ref. 41) or Sun *et al.* (275.73).[42] The difference may be explained by the fact that their results were obtained for microcrystalline rather than nanocrystalline diamond. However, although consideration of changes in the phonon lifetime of nanocrystals leads to a better agreement between theoretical and experimental Raman data [Fig. 3(a)], the discrepancies remain fairly large.

D. Size distribution in nanodiamond powders

The ND powders analyzed in this study contain diamond crystals with sizes ranging from 3 to 30 nm.[35] While the majority of the nanocrystals were between 4 and 5 nm, the Raman scattering cross section is proportional to the crystal volume and is thus much larger for larger crystals. On the other hand, confinement effects, such as the asymmetric peak broadening, are more distinct for small crystals (<10 nm). Therefore, experimentally obtained Raman spectra are expected to contain Raman features from both small and large ND crystals. Their simultaneous contribution to the total Raman intensity leads to a complex shape that cannot be fitted using a single peak in the PCM.

Figure 4 shows the calculated diamond Raman peaks (normalized intensities) of 3-, 3.3-, and 7-nm ND crystals, in comparison to a sample that contains a mixture of 3- and 7-nm crystals (ratio 12:1, average crystal size is 3.3 nm), each contributing equally to the overall intensity. The Raman signal of a 3-nm crystal is more than 12 times weaker than that of a 7-nm ND crystal due to the volume dependence of the Raman intensity. Thus, although the relative amount of large ND crystals in the sample is small, their contributions to the overall Raman intensity cannot be neglected. The superposition of the Raman intensities of small and large crystals leads to a Raman peak different from that computed for the average crystal size (3.3 nm). In order to account for the complex peak shape resulting from simultaneous contributions of different crystal sizes, we fitted the Raman spectra of the oxidized powders using two separate peaks, with Peak 1 and Peak 2 representing smaller and larger ND crystals, respectively [Fig. 5(a)]. Changes in L and Γ upon oxidation are shown in Fig. 5(b). Both Raman peaks indicate a nonlinear increase in L with increasing oxidation time following Eq. (3). The corresponding parameters are $C_1=-9.0\cdot10^{-4}$ nm/h^2, $C_2=0.07$ nm/h, and $C_3=4.5$ nm for Peak 1 and $C_1=-2.1\cdot10^{-3}$ nm/h^2, $C_2=0.16$ nm/h, and $C_3=9.4$ nm for Peak 2.

Γ decreases linearly and can be approximated by Eq. (5), where D_1 and D_2 were found to be -0.08 cm^{-1}/h and 32.2 cm^{-1} for Peak 1, and -0.04 cm^{-1}/h and 15.0 cm^{-1} for Peak 2. The relationship between L and Γ is plotted in Fig. 5(c). It can be seen that Eq. (4) (Fit 1), used for the fit in Fig. 3, results in a rather poor agreement with the computed data. A better agreement (Fit 2) is achieved using the relation

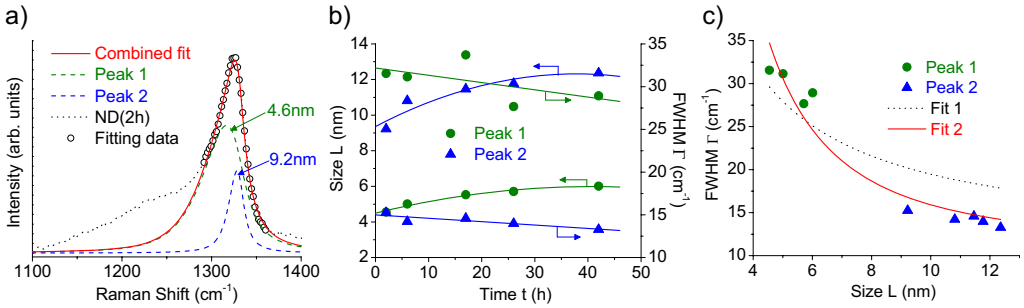

FIG. 5. (Color online) (a) Raman spectrum of oxidized ND (2 h at 430 °C) fitted using two peaks in order to account for small and large ND crystals. A similar fitting procedure was used for all oxidized ND powders in order to determine (b) changes in Γ and L as a function of oxidation time and (c) the relationship between both fitting parameters.

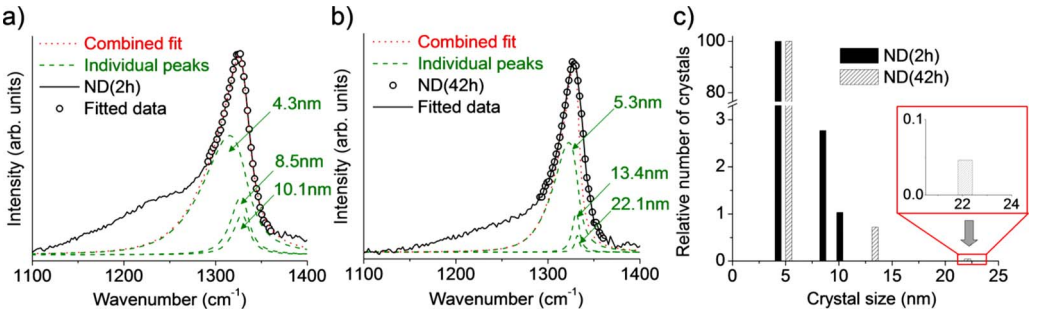

FIG. 6. (Color online) Raman spectra of ND oxidized for 2 h (a) and 42 h (b) fitted using three individual peaks. The size distribution (c) was determined by correcting the Raman intensity of the individual crystal sizes for differences in crystal volume.

$$\Gamma = A + \frac{B}{L^2}. \tag{6}$$

The parameter A was set to 11.0 cm^{-1}. The value of B was found as 491.25 cm^{-1} nm^2.

Therefore, accounting for the broad size distribution of ND powders leads to a better agreement between the calculated and experimental Raman data [compare Figs. 2(b) and 5(a)]. Considering the volume dependence of the Raman intensity, one can potentially estimate the contribution of various crystal sizes to the total Raman intensity and determine the size distribution in the ND powders. Figures 6(a) and 6(b) show the Raman spectra of ND oxidized for 2 and 42 h, respectively. Both spectra were fitted using three individual peaks. The corresponding crystal sizes were 4.3, 8.5, and 10.1 nm for ND(2h) and 5.3, 13.4, and 22.1 nm for ND(42h). The relative number of ND crystals was determined by correcting the Raman intensity of each peak for the crystal volume. The resulting size distribution is shown in Fig. 6(c). It can be seen that the size distribution broadens with increasing oxidation time and the average crystal size is shifted toward higher values, in agreement with the results obtained from HRTEM and XRD studies.[35]

E. Phonon dispersion and lattice defects

Previous studies on phonon confinement in nanocrystals did not account for possible contributions from lattice defects. However, L represents the coherence length and is therefore a measure of the distance between dislocations, twin boundaries, stacking faults, vacancies, interstitials, impurities, and other defects within the crystal lattice. The assumption that L represents the crystal size is only valid for defect-free crystals, where the surface limits the propagation of the phonons. This assumption does not hold for imperfect crystals produced by detonation methods, which contain twins and other defects as shown in Fig. 7. As a consequence, the coherence length L becomes significantly smaller than the actual ND crystal size.

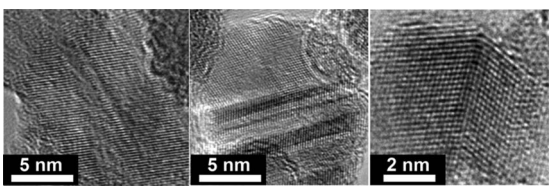

FIG. 7. HRTEM images of ND crystals. Detonation ND crystals exhibit lattice defects such as twins and dislocations which affect phonon propagation.

Therefore, while the results above were produced assuming the ND crystal to be larger than 3 nm ($L>3$ nm), we now allow vibrational domains (coherence lengths) with $L<3$ nm to contribute to the Raman spectrum. In addition, the frequency range used for fitting is extended to 1100–1400 cm^{-1}. The fitting results for ND(2h) are shown in Fig. 8(a). Two peaks have been used for the analysis. It can be seen that the agreement between calculated and measured Raman spectra is significantly improved and the broad shoulder (<1300 cm^{-1}) can now be well fitted using this approach [Fig. 8(a)]. The corresponding L (and Γ) for Peak 1 and Peak 2 are 6.45 nm (15.6 cm^{-1}) and 2.67 nm (84.8 cm^{-1}), respectively. Changes in L and Γ upon oxidation are shown in Fig. 8(b). Peak 1 corresponds to L values in the range 6–8 nm and may be assigned to defect-free 6–8 nm ND crystals or to defective larger ND crystals (>8 nm). The L values obtained from Peak 2 are significantly smaller and range between 2.6 and 3.7 nm. Assuming the majority of the ND crystals to be 4–8 nm in size, a coherence length of 2–4 nm may suggest one to two defects per ND crystal. While this is in good agreement with HRTEM studies, the reported numbers merely represent the average values. Defect-free ND crystals of similar size and crystals with three or more defects have also been observed.

Ager *et al.*[29] and Yoshikawa *et al.*[41] estimated the crystal size using an averaged one-dimensional dispersion curve.

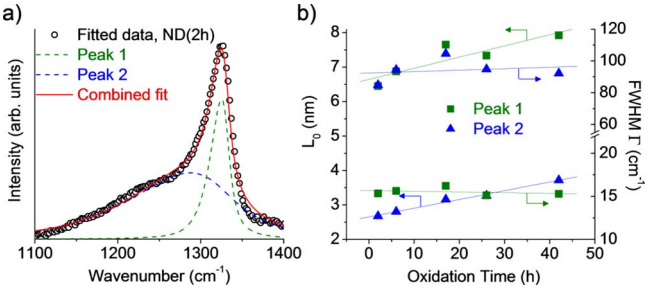

FIG. 8. (Color online) (a) Raman spectrum of oxidized ND (2 h at 430 °C) fitted using two peaks. (b) Changes in L and Γ with increasing oxidation time.

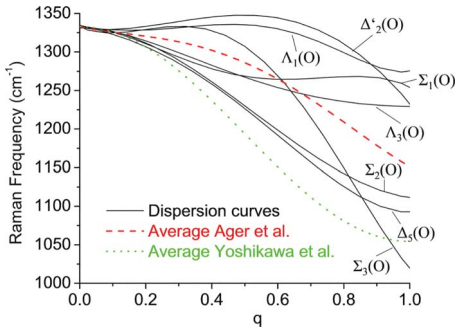

FIG. 9. (Color online) Energy dispersion of phonon modes in diamond after Pavone *et al.* (see Ref. 43).

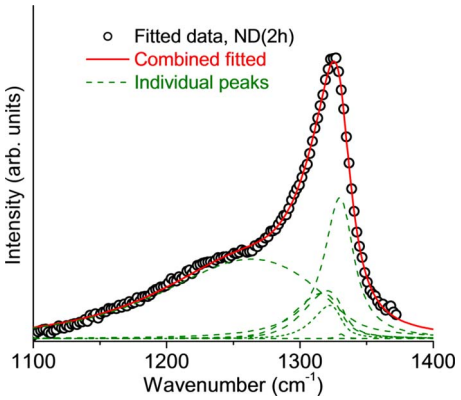

FIG. 10. (Color online) Raman spectrum of oxidized ND (2 h at 430 °C) fitted using seven peaks, each representing the contribution of one dispersion relation.

However, while this approximation is justified for small phonon wave vectors $q<0.1$, it oversimplifies the energy dispersion of the phonon modes for larger q. A coherence length of 2.6 nm would allow phonons with $q>0.1$ to contribute to the Raman signal. As $\Delta q=\pi/L$, an average crystal size of 4 nm leads to a phonon wave vector uncertainty of approximately $\Delta q\approx 0.09$ with respect to the size of the BZ. Therefore, while the dispersion relation of Yoshikawa *et al.*[41] can be used for $L=4$ nm, coherence lengths below 3 nm require a more accurate description of the energy dispersion of the individual phonon branches, in particular for $q>0.1$. Moreover, it should be noted that the relation $\Delta q=\pi/L$ underestimates the uncertainty for strongly confined phonons and phonons with larger q values may contribute to the Raman spectra, requiring a more accurate consideration of the phonon energy dispersion relations.

In this study, we used the calculated dispersion relations from Pavone *et al.*[43] (Fig. 9), which are in good agreement with the experimental data obtained so far. The optical phonon branches of the [110], [001], and [111] direction are referred to as Σ, Δ, and Λ, respectively, following the notation of Warren *et al.*[44,45] and plotted in Fig. 9. The individual phonon branches were fitted using polynomial functions of the type

$$\omega(q) = A + B \cdot q + C \cdot q^2 + D \cdot q^3 + E \cdot q^4 + F \cdot q^5. \quad (7)$$

The corresponding coefficients *A*-*F* are shown in Table I. It is important to mention that the absolute values for q vary for the Σ, Δ, and Λ directions. The size of the BZ depends on the lattice spacing and is therefore different for the [110], [100], and [111] directions.

Figure 9 suggests that only Δ_5(O) and Σ_2(O) branches with $q\sim 0.4$, and Σ_3(O) and Λ_3(O) branches with $q\sim 0.6$ exhibit phonon frequencies that can contribute to the broad shoulder around 1200–1300 cm^{-1}. The crystal sizes needed to provide the required uncertainty in the phonon wave vector are smaller than the actual ND crystals ($L>4$ nm, $q<0.1$). However, as discussed above, L may be significantly smaller than the actual crystal size. In order to account for defect contributions and the energy dispersion of the phonon branches we fitted the Raman spectrum of ND(2h) using seven peaks, each attributed to one of the individual phonon branches in Fig. 9. The peak parameters were computed using the approach of Yoshikawa *et al.*[41] and the dispersion relations from Table I. The results are shown in Fig. 10. A good agreement between calculated and measured Raman data suggests that phonon wave vectors from small vibrational domains can indeed be responsible for the broad shoulder at 1250 cm^{-1} typically observed in the Raman spectra of ND powders. The corresponding L values are shown in Table II. It should be noted that since the size of the BZ depends on the crystalline direction, the lattice-constant a for the Δ, Σ, and Λ directions is given by 0.357, 0.252, and 0.206 nm, respectively. In the computations above, each L is only represented by one phonon branch for simplicity reasons. Adding the contributions of the remaining six phonon

TABLE I. Coefficients of the polynomial fitting functions used to describe the energy dispersion of the individual phonon branches.

	A (cm^{-1})	B (cm^{-1})	C (cm^{-1})	D (cm^{-1})	E (cm^{-1})	F (cm^{-1})
Λ_1	1332.41	−48.68	52.92	820.93	−1940.67	1057.13
Λ_3	1332.69	15.89	−774.82	1478.03	−1238.23	415.97
Δ_2	1332.48	−113.54	873.49	−1700.98	1290.34	−449.49
Δ_5	1332.81	51.63	−1381.23	3135.02	−3670.5	1626.12
Σ_3	1332.13	−184.58	1382.08	−2935.51	1424.39	0
Σ_1	1332.02	13.66	−892.48	1639.97	−838.27	0
Σ_2	1332.19	−35.25	−393.37	33.21	175.23	0

TABLE II. Calculated coherence lengths for the phonon branches shown in Fig. 9.

	L (in units of a)	L (in nm)
Λ_1	54.7	11.3
Λ_3	12.3	2.5
Δ_2	48.9	17.4
Δ_5	5.2	1.9
Σ_3	7.3	1.8
Σ_1	11.5	2.9
Σ_2	15.5	3.9

branches for each L value leads to a further improvement of the fit. Although these peaks would have a physical meaning, computations using all 49 peaks are more time consuming, and lead only to a slight improvement.

Although the described approach appears to be more complex compared to Ager's and Yoshikawa's, it provides an explanation for the broad shoulder centered at 1250 cm^{-1} and may also give an estimate on the number of defects in the ND crystals. Moreover, once coded, the model can be easily incorporated into standard spectroscopy software and used by an operator routinely.

F. Limitations of the PCM

Although the agreement between experimentally obtained and calculated Raman spectra has been significantly improved by taking in consideration the crystal size distribution and presence of lattice defects, some limitations remain. The arguably most significant oversimplification of the PCM stems from the assumption that nanocrystals of 3–20 nm in size, showing extensive surface reconstruction and lattice defects, are assumed to have the phonon density of states of bulk diamond. Moreover, further research will be required to measure strain and understand its effects on the Raman spectra of individual nanocrystals. Changes in lattice constants, as a consequence of confinement and minimization of Gibbs free energy, have also been reported for nanocrystals. However, their effect on vibrational frequencies and phonon lifetimes still remains underexplored.

IV. CONCLUSIONS

Confinement-related changes in the Raman spectra of ND were used to estimate the crystal size in different ND powders with average crystal sizes in the range 4–7 nm. While the PCM was successfully used to accurately measure the size of Si and GaAs nanocrystals, quantitative size characterization remains a challenge in the case of ND powders due to the complexity of their Raman spectra. However, using a computational approach and taking into consideration lattice defects, and size distributions, good agreement between the theoretical predictions of the PCM and experimental Raman data has been achieved. HRTEM and XRD were used as complementary techniques in order to correctly interpret Raman data and to support the obtained results. While the modified PCM can be incorporated in Raman analysis software, allowing for a fast and straightforward size characterization of nanodiamond powders, further research is needed to improve the reliability of the model. In particular, a better understanding of the phonon density of states of highly complex structures such as nanodiamond crystals is required for accurate quantitative Raman characterization.

ACKNOWLEDGMENTS

The authors are grateful to Nanoblox, Inc. for providing the ND powder. We thank J. E. Fischer (University of Pennsylvania), P. Scharff (Ilmenau University of Technology, Germany), C. Li, R. Schweitzer-Stenner, and J. Spanier (all at Drexel University) for helpful discussions. The Centralized Research Facility at Drexel University's College of Engineering provided access to spectrometers used in this study. This work was partially supported by the Pennsylvania Nanotechnology Institute (NTI) through Ben Franklin Technology Partners of Southeastern Pennsylvania.

*Present address: Department of Materials Science and Engineering, Massachusetts Institute of Technology, Cambridge, Massachusetts 02139, USA.

†Present address: ARKEMA - Groupement de Recherches de Lacq, Groupe NTC - B.P. 34 - 64170 Lacq, France.

‡Corresponding author. FAX: +1-215-895-1934; gogotsi@drexel.edu

[1] Y. Gogotsi, *Carbon Nanomaterials* (CRC Press, Boca Raton, Florida, 2006).

[2] A. C. Ferrari and J. Robertson, Philos. Trans. R. Soc. London, Ser. A **362**, 2269 (2004).

[3] *Raman Scattering in Materials Science*, edited by W. H. Weber and R. Merlin (Springer, Berlin, New York, 2000).

[4] H. A. Szymanski, *Raman Spectroscopy: Theory and Practice* (Pergamon Press, New York, 1964).

[5] D. A. Long, *Raman Spectroscopy* (McGraw-Hill, New York, 1977).

[6] Y. Kawashima and G. Katagiri, Phys. Rev. B **52**, 10053 (1995).

[7] C. Thomsen and S. Reich, Phys. Rev. Lett. **85**, 5214 (2000).

[8] D. S. Knight and W. B. White, J. Mater. Res. **4**, 385 (1989).

[9] S. Prawer and R. J. Nemanich, Philos. Trans. R. Soc. London, Ser. A **362**, 2537 (2004).

[10] A. C. Ferrari and J. Robertson, Phys. Rev. B **63**, 121405(R) (2001).

[11] V. Mochalin, S. Osswald, and Y. Gogotsi, Chem. Mater. **21**, 273 (2009).

[12] C. Kittel, *Introduction to Solid State Physics* (Oldenbourg Verlag Muenchen, Wien, 2002).

[13] *Fullerenes, Semiconductor Surfaces, Coherent Phonons*, edited by M. Cardona and G. Güntherodt, Light Scattering in Solids

Vol. 8 (Springer, Berlin, New York, 2000).
[14] R. J. Nemanich, S. A. Solin, and R. M. Martin, Phys. Rev. B **23**, 6348 (1981).
[15] H. Richter, Z. P. Wang, and L. Ley, Solid State Commun. **39**, 625 (1981).
[16] P. Verma, W. Cordts, G. Irmer, and J. Monecke, Phys. Rev. B **60**, 5778 (1999).
[17] E. Duval, Phys. Rev. B **46**, 5795 (1992).
[18] A. K. Arora, M. Rajalakshmi, T. R. Ravindran, and V. Sivasubramanian, J. Raman Spectrosc. **38**, 604 (2007).
[19] I. H. Campbell and P. M. Fauchet, Solid State Commun. **58**, 739 (1986).
[20] P. M. Fauchet and I. H. Campbell, CRC Crit. Rev. Solid State Mater. Sci. **14**, s79 (1988).
[21] J. Gonzalez-Hernandez, G. H. Azarbayejani, R. Tsu, and F. H. Pollak, Appl. Phys. Lett. **47**, 1350 (1985).
[22] G. Braunstein, D. Tuschel, S. Chen, and S. T. Lee, J. Appl. Phys. **66**, 3515 (1989).
[23] K. K. Tiong, P. M. Amirtharaj, F. H. Pollak, and D. E. Aspnes, Appl. Phys. Lett. **44**, 122 (1984).
[24] A. C. Ferrari and J. Robertson, Philos. Trans. R. Soc. London, Ser. A **362**, 2477 (2004).
[25] O. O. Mykhaylyk, Y. M. Solonin, D. N. Batchelder, and R. Brydson, J. Appl. Phys. **97**, 074302 (2005).
[26] E. D. Obraztsova, K. G. Korotushenko, S. M. Pimenov, V. G. Ralchenko, A. A. Smolin, V. I. Konov, and E. N. Loubnin, Nanostruct. Mater. **6**, 827 (1995).
[27] S. Osswald, G. Yushin, V. Mochalin, S. Kucheyev, and Y. Gogotsi, J. Am. Chem. Soc. **128**, 11635 (2006).
[28] G. N. Yushin, S. Osswald, V. I. Padalko, G. P. Bogatyreva, and Y. Gogotsi, Diamond Relat. Mater. **14**, 1721 (2005).
[29] J. W. Ager, D. K. Veirs, and G. M. Rosenblatt, Phys. Rev. B **43**, 6491 (1991).
[30] H. Boppart, J. van Straaten, and I. F. Silvera, Phys. Rev. B **32**, 1423 (1985).
[31] S. S. Mitra, O. Brafman, W. B. Daniels, and R. K. Crawford, Phys. Rev. **186**, 942 (1969).
[32] M. H. Grimsditch, E. Anastassakis, and M. Cardona, Phys. Rev. B **18**, 901 (1978).
[33] M. J. Lipp, V. G. Baonza, W. J. Evans, and H. E. Lorenzana, Phys. Rev. B **56**, 5978 (1997).
[34] M. Yoshikawa, Y. Mori, H. Obata, M. Maegawa, G. Katagiri, H. Ishida, and A. Ishitani, Appl. Phys. Lett. **67**, 694 (1995).
[35] S. Osswald, M. Havel, V. Mochalin, G. Yushin, and Y. Gogotsi, Diamond Relat. Mater. **17**, 1122 (2008).
[36] B. Palosz, in *Nanodiam*, edited by S. Mitura, P. Niedzielski, and B. Walkowiak (Wydawnictwo Naukowe, Warszawa, 2006), p. 129.
[37] V. Mochalin, S. Osswald, C. Portet, G. Yushin, C. Hobson, M. Havel, and Y. Gogotsi, Mater. Res. Soc. Symp. Proc. **1039**, 1039-P11-03 (2008).
[38] S. Osswald, E. Flahaut, H. Ye, and Y. Gogotsi, Chem. Phys. Lett. **402**, 422 (2005).
[39] S. Osswald, E. Flahaut, and Y. Gogotsi, Chem. Mater. **18**, 1525 (2006).
[40] S. Osswald, K. Behler, and Y. Gogotsi, J. Appl. Phys. **104**, 074308 (2008).
[41] M. Yoshikawa, Y. Mori, M. Maegawa, G. Katagiri, H. Ishida, and A. Ishitani, Appl. Phys. Lett. **62**, 3114 (1993).
[42] Z. Sun, J. R. Shi, B. K. Tay, and S. P. Lau, Diamond Relat. Mater. **9**, 1979 (2000).
[43] P. Pavone, R. Bauer, K. Karch, O. Schütt, S. Vent, W. Windl, D. Strauch, S. Baroni, and S. de Gironcoli, Physica B **219-220**, 439 (1996).
[44] J. L. Warren, J. L. Yarnell, G. Dolling, and R. A. Cowley, Phys. Rev. **158**, 805 (1967).
[45] J. L. Warren, R. G. Wenzel, and J. L. Yarnell, *Inelastic Scattering of Neutrons* (International Atomic Energy Agency, Vienna, 1965), p. 361.